Fiori *et al. Earth, Planets and Space* (2016) 68:100
DOI 10.1186/s40623-016-0472-7

Earth, Planets and Space

FULL PAPER Open Access

Calibration and assessment of Swarm ion drift measurements using a comparison with a statistical convection model

R. A. D. Fiori[1*], A. V. Koustov[2], D. H. Boteler[1], D. J. Knudsen[3] and J. K. Burchill[3]

Abstract

The electric field instruments onboard the Swarm satellites make high-resolution measurements of the F-region ion drift. This paper presents an initial investigation of preliminary ion drift data made available by the European Space Agency. Based on data taken during polar cap crossings, we identify large offsets in both the along-track and cross-track components of the measured ion drift. These offsets are removed by zeroing drift values at the low-latitude boundary of the high-latitude convection pattern. This correction is shown to significantly improve agreement between the Swarm ion drift measurements and velocity inferred from a radar-based statistical convection model for periods of quasi-stability in the solar wind and interplanetary magnetic field. Agreement is most pronounced in the cross-track direction ($R = 0.60$); it improves slightly ($R = 0.63$) if data are limited to periods with IMF $B_z < 0$. The corrected Swarm data were shown to properly identify the convection reversal boundary for periods of IMF $B_z < 0$, in full agreement with previous radar and satellite measurements, making Swarm ion drift measurements a valuable input for ionospheric modeling.

Keywords: Ion drift, Swarm electric field instrument, Ionospheric plasma flow

Introduction

The Swarm satellite mission is aimed at providing a survey of the geomagnetic field and a global representation of its variation on timescales from hours to years (Friis-Christensen et al. 2006, 2008). To help resolve the different sources of magnetic variations, it is important to map the ionospheric contribution. One of the principal objectives of the mission is therefore an investigation of the electric currents flowing in the magnetosphere and ionosphere. To help achieve this objective, each Swarm satellite carries an electric field instrument (EFI) that measures the ion drift (driven by the ionospheric electric and magnetic fields) at a high spatial resolution along the satellite track, to provide information on the structure of the currents at the ionospheric level.

Fiori et al. (2013, 2014) have investigated techniques for estimating 2D plasma convection in the high-latitude ionosphere using Swarm data. They showed that Swarm data can be incorporated into a spherical cap harmonic mapping algorithm that generates high-latitude convection maps from ground-based radar data. In both papers, data sets were artificially generated by considering statistical models to emulate ion drift measurements along hypothetical Swarm satellite tracks. It was shown that Swarm-based measurements could successfully map convection both over a localized region surrounding the satellite track (to examine small scale features) and across the entire high-latitude region when combined with data from the Super Dual Aurora Radar Network (SuperDARN) radars (Greenwald et al. 1995; Chisham et al. 2007). The logical progression of this work is the testing of Swarm measurements, the comparison of Swarm data with plasma flow measurements from other instruments to ensure the data sets are suitable for merging, and finally the generation of convection maps.

*Correspondence: robyn.fiori@canada.ca
[1] Geomagnetic Laboratory, Natural Resources Canada, 2617 Anderson Road, Ottawa, ON K1A 0E7, Canada
Full list of author information is available at the end of the article

An initial release of Swarm EFI data (PREL 0101, available at https://earth.esa.int/web/guest/swarm/data-access) has been made publically available for the period of April 15, 2014, to September 29, 2014. The calibration of data in this initial release is based primarily on numerical modeling of the instruments and on limited comparisons with data taken in flight. As shown below, these data are subject to large offsets, the source of which is not yet fully understood. One possible source is time variation of the gain distribution over the 2D detector surface; the cause of which is suspected to be contamination from residual humidity absorbed prior to flight [R. Enck, personal communication]. This gain variation changes on timescales of tens of minutes in the case of the Swarm C satellite, and hours or weeks in the case of Swarm A and B, with Swarm A being the most stable. While such gain variations clearly compromise the accuracy of the EFI measurements, the relative stability of the gain patterns over one orbit provides an opportunity to calibrate the measurements on an orbit-by-orbit basis, based on the assumption of relatively low convection velocity at subauroral latitudes. This approach has been used in preliminary studies of high-latitude flow channels (Goodwin et al. 2015; Archer et al. 2015).

The concept of low-to-zero flow at subauroral latitudes has been applied to mapping electrostatic potential patterns derived from ion drift and electric field measurements from satellites. In deriving large-scale statistical convection patterns from Defence Meteorological Satellite Program (DMSP) ion drift data, Rich and Hairston (1994) developed a detailed algorithm for setting the electrostatic potential to zero just equatorward of the auroral oval. They characterized the location of the subauroral region based on the observation of a constant near-zero ion flow in both the along-track and cross-track directions having a sufficiently small standard deviation located equatorward of 65° magnetic latitude (MLAT). The potential calculated at the located end point was used as an offset to correct the potential calculated along the entire high-latitude portion of the satellite pass. Weimer (1995) also pointed out the need to correct for unknown offsets in Dynamics Explorer 2 (DE2) electric field data. For each satellite pass he identified reference points, chosen to be the low-latitude boundary of the convection zone, where the potential should be the same. If reference point potentials did not match, offsets were introduced into the electric field data to ensure a match. Similar techniques are applied by Hairston and Heelis (1990) for DE 2 data and by Hairston and Heelis (1995) for DMSP data. Zeroing the potential at the low-latitude convection zone boundary, according to Weimer (1995), allows one to isolate the solar wind-driven component of the potential pattern. It should be noted that zeroing the potential at lower latitudes is equivalent to applying an offset to the velocity data to set it to zero.

In this paper, we empirically correct Swarm ion drift measurements by zeroing the flow magnitude at the boundary of the convection zone inferred from a SuperDARN-based statistical convection model. Corrections are only applied to data poleward of the convection zone boundary. The corrected ion drift measurements are then compared to values predicted by the model. The goal of this comparison is to determine whether or not corrected Swarm ion drift data provide a more accurate representation of the average ion drift at high latitudes than measured data. Finally, we investigate the location of the convection reversal boundary inferred from Swarm data with respect to its statistically determined average location known from SuperDARN measurements.

EFI instrument onboard the Swarm satellites

The electric field instrument (EFI) (Knudsen et al. 2016) consists of four sensors: two orthogonal bi-dimensional thermal ion imagers (TIIs) and two Langmuir probes (LPs). The TII sensors, which view in the horizontal and vertical planes, are used to construct a two-dimensional low-energy ion distribution function to derive ion temperature (T_{ion}) and three-dimensional ion drift values (Knudsen et al. 2003).

This study makes use of EFI ion drift data obtained from May to September 2014; Swarm data prior to May 2014 were subject to 'measurements jitter' due to problems with the EFI TII flight software (Knudsen et al. 2015). Only data from the Swarm A satellite are used in this study. Following the recommendation of Knudsen et al. (2015) Swarm data associated with a TII quality flag $\geq$20 are removed from the data set. Additionally, points having T_{ion} of <100 K or a measured along-track ion drift component of 0 m/s were removed as these data are not consistent with the overall data set. Swarm A data are available for 142 days over the May–September 2014 interval.

Swarm measures ion drift in the along-track and cross-track directions independently by the two TII sensors. The horizontal (H) sensor measures the along-track (H_{x}) and cross-track (H_{y}) components of the ion drift, and the vertical (V) sensor measures the along-track (V_{x}) and vertical components of the ion drift. Ion drift values are transformed into the North East Center (NEC) reference frame for data distribution. The NEC frame has its origin at the front of the satellite in the vicinity of the EFI (Swarm Team 2004). The radial (C) direction is oriented to point from the origin to the center of the Earth. The north (N) and east (E) components point to the north and east directions, respectively. It should be pointed out that H_x, V_x, and H_y point approximately in the cross-track

directions; attitude swings of up to ±4° are not corrected for in these measurements. We also note that in this version of the data release, the ion temperature calibration is based primarily on a numerical simulation of the TII sensors and has not yet undergone any adjustment based on post-launch data. Data for a single satellite pass will be discussed later in "Comparison of corrected Swarm data: Single Satellite Pass (04 July 2014)" section (see Fig. 2).

The reader will note that H_x and V_x measure the same ion drift component. However, visual examination of the data from numerous high-latitude satellite passes during the May–September interval found that in many instances H_x and V_x did not agree; discontinuities (sharp jumps of several thousand m/s) were frequently observed in data from the horizontal sensor but not the vertical sensor. Although such jumps could be real, the lack of corroborating data from the parallel sensor puts the validity of the data into question, and the horizontal data in this case are treated as erroneous. On some occasions jumps were observed in the vertical sensor instead of the horizontal sensor. Jumps appear mainly at MLTs and MLATs in the vicinity of the cusp region, but at present their cause is not understood. In assessing satellite passes for the comparison study, disagreement between the along-track components from the horizontal and vertical TII sensors was considered. Passes showing extreme disagreement were flagged so that data from only one sensor were used to determine the along-track ion drift measurement. If data for both sensors did not contain discontinuities and followed the same trends, then the data were averaged.

For the purpose of convection mapping, we are only interested in intervals where the Swarm satellite is located in the high-latitude region poleward of the convection zone boundary, as defined in the magnetic coordinate system. Swarm data coordinates and vector orientations are therefore transformed to the altitude-adjusted corrected geomagnetic (AACGM) coordinate system (Baker and Wing 1989; Bhavnani and Hein 1994). In addition, the measured ion drifts are mapped down from a satellite altitude of ~470–300 km, which is the assumed height of SuperDARN F-region scatter (i.e., Koustov et al. 2007; Chisham et al. 2008). The effect of this is to reduce the magnitude of the ion drift measurement by ~4 %, as estimated using the methods of Walker and Sofko (2015). Data are further resampled from a 2-Hz resolution to 1 Hz by discarding every other point simply to reduce the data set for ease of calculation. For comparison purposes, we focus on northern hemisphere data.

Swarm satellites complete a full orbit approximately 16 times per day, spending ~20 min of each orbit in the high-latitude region poleward of 50° MLAT in the northern hemisphere. Figure 1a shows the distribution of the coordinates for the Swarm A satellite tracks for all available northern hemisphere passes in the May–September 2014 interval. Occurrence is plotted in magnetic latitude/magnetic local time (MLAT/MLT) coordinates using a uniform distribution of equal area cells having a length equivalent to 1° of MLAT. As expected, the distribution is more concentrated in the high-latitude region due to the satellite's polar orbit. Data are weighted toward the dayside as the satellite orbits about the geographic pole,

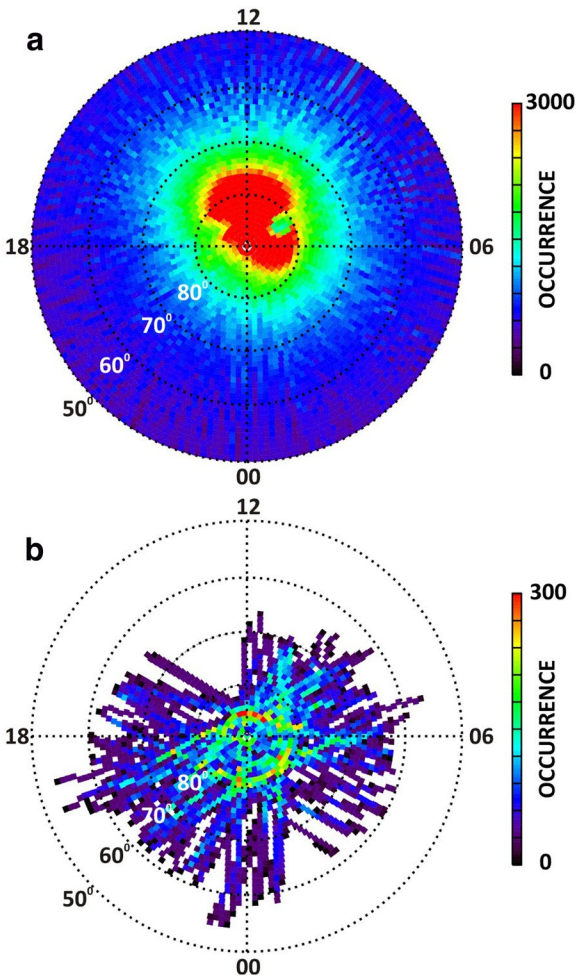

Fig. 1 Distribution of Swarm A satellite footprints. **a** Distribution of the coordinates of the satellite track for the Swarm A satellite for all available passes May–September 2014. Number of measurements (occurrence) is indicated by *color* using a uniformly distributed grid of equal area cells in the high-latitude (>50° MLAT) region of the northern hemisphere in MLAT/MLT coordinates. Each grid cell has a length equivalent to 1° of MLAT. **b** Same as (**a**), but for a subset of 70 passes for periods of quasi-stable IMF and solar wind. Data are limited to the convection zone, determined by finding the intersection of the footprints of the satellite orbit with the Heppner–Maynard Boundary (HMB) corresponding to the Cousins and Shepherd (2010) statistical model for that period (see descriptions in "Statistical convection model" section)

and during this time interval the northern hemisphere is predominantly tilted toward the sun.

Comparison of Swarm data with output from a statistical convection model

We now compare Swarm data with predictions of the high-latitude plasma flow velocity given by a statistical convection model to evaluate the offset between values and to evaluate the success of our proposed procedure for removing the offset.

Statistical convection model

Over the years, several statistical models of the high-latitude convection pattern have been generated based on ionospheric data from a variety of both satellite and ground-based instruments. These instruments include drift meters on satellites (Hairston and Heelis 1990; Papitashvili et al. 1999; Rich and Hairston 1994; Papitashvili and Rich 2002), vector electric field instruments on satellites (Heppner and Maynard 1987; Rich and Maynard 1989; Weimer 1995), incoherent scatter radar (Foster et al. 1986; Zhang et al. 2007), and the SuperDARN coherent scatter radars (Ruohoniemi and Greenwald 1996, 2005; Cousins and Shepherd 2010; Pettigrew et al. 2010). Of these models, we selected the CS10 convection model by Cousins and Shepherd (2010) because of its flexibility, accessibility, and well-defined parameterization of the convection pattern by the solar wind velocity and the strength and orientation of the interplanetary magnetic field (IMF).

The CS10 statistical convection model is derived from data collected by 16 SuperDARN radars operating over a period of 8 years. There are 270 models categorized by hemisphere, transverse IMF clock angle $\left(\alpha = a\tan\left(\frac{B_y}{B_z}\right)\right)$, magnitude of the solar wind electric field ($\boldsymbol{E_{sw}} = -\boldsymbol{v_{sw}} \times \boldsymbol{B_t}$, where $\boldsymbol{v_{sw}}$ is the solar wind velocity, $|\boldsymbol{B_t}| = \sqrt{\left(B_y^2 + B_z^2\right)}$ is the transverse component of the IMF, and B_y and B_z are the y and z-components of the IMF), and dipole tilt angle (β) of the Earth's magnetic field. Note that the geocentric solar magnetospheric (GSM) coordinate system is used to describe the IMF and solar wind. Each map is generated by fitting collected data in each bin using a modified spherical harmonic fitting procedure called the FIT technique (Ruohoniemi and Baker 1998; Shepherd and Ruohoniemi 2000). The model output is a set of coefficients from which velocity, and, if desired, electrostatic potential may be calculated at any point within the high-latitude region.

The FIT technique requires that a high-latitude convection zone be defined such that the flow is zero at the low-latitude boundary. This boundary, defined by latitude λ_{FIT}, is determined based on the distribution and magnitude of the binned line-of-sight velocities by selecting the lowest latitude containing all gridded line-of-sight velocities greater than 100 m/s (Ruohoniemi and Baker, 1998). For the 270 possible CS10 models, λ_{FIT} ranges from 52° MLAT to 66° MLAT with an average value of 60° MLAT. The convection zone is further shaped by imposing a Heppner–Maynard Boundary (HMB) (Heppner and Maynard 1987; Shepherd and Ruohoniemi 2000) which is compressed on the dayside and circular on the nightside. An HMB is applied to the data set by filling grid cells in the region between λ_{FIT} and the HMB with fill vectors having magnitudes of 1 m/s to damp the flow.

In describing ionospheric convection, it is common to differentiate between flow patterns associated with southward ($B_z < 0$) IMF, where there is strong coupling between the IMF and the geomagnetic field, and northward IMF ($B_z > 0$). For periods of southward IMF, convection is two-celled with one cell located on the dawnside and the other on the duskside (Dungey 1961). Flow is in general directed anti-sunward (from noon-to-midnight) at the highest latitudes over the polar cap, closed by sunward-directed flow (from midnight-to-noon) at more equatorward latitudes on the dawnside and duskside. For periods of northward IMF, the convection pattern tends to be multi-celled; the two cells characterizing periods of southward IMF are compressed toward the nightside and joined by 1–2 reverse convection cells on the dayside, characterized by sunward-directed flow over the polar cap (e.g., Reiff and Burch 1985; Watanabe and Sofko 2009). The size and orientation of convection cells, and the strength of the overall convection pattern are dependent on the same parameters that are used to bin the statistical models (e.g., Cowley and Lockwood 1992; Zhang et al. 2007 and references therein).

In the following sections, attempts are made to correct the Swarm ion drift measurements by determining and removing offsets. The CS10 statistical model represents the ionospheric convection during periods of stable IMF and solar wind. Comparison between Swarm ion drift measurements and the CS10 statistical models must therefore be performed during periods where the IMF and solar wind parameters used for binning the CS10 statistical models are quasi-stable. This is necessary to ensure the ionospheric convection pattern itself is not in a period of transition so that the correct CS10 statistical model pattern can be used for comparison. In addition, the requirement of quasi-stability reduces possible errors due to the inaccurate propagation of the solar wind and IMF parameters from the L1 point, where they are measured, to the Earth.

Identifying periods of quasi-stable solar wind and IMF

To define periods of quasi-stability in the solar wind and IMF, we use methods similar to those outlined by Shepherd et al. (2002). Measurements of the solar wind and IMF parameters, necessary for selecting the correct statistical model, are taken from the OMNI database (http://nssdc.gsfc.nasa.gov/omniweb/), which propagates solar wind and IMF measurements from the point of measurement to the subsolar point of the bow shock using the Weimer technique (Weimer and King, 2008) to provide values for the solar wind and IMF near the outer boundary of the magnetosphere. OMNI data are processed to create 10-min data averages and then examined to determine periods where criteria for quasi-stability are met. Quasi-stability is defined as a period where B_y, B_z, and E_{sw} for three or more consecutive 10-minute averages are such that $\frac{|\Delta x|}{x} < 5\,\%$, where x represents the parameter tested (B_y, B_z, E_{sw}) and Δx is the difference between the minimum and maximum values of x. The first and last 10-minute intervals are dropped to allow for a $\pm$ 10 min uncertainty in the propagation time and to allow for the reconfiguration of the ionospheric convection pattern following an IMF transition (e.g., Shepherd et al. 2002; Cousins and Shepherd 2010).

Once periods of quasi-stability have been determined, it is possible to examine how the Swarm ion drift data compares to velocities obtained from the statistical convection model.

Data selection and preprocessing

The quasi-stable intervals identified were examined for the presence of complete passes of the Swarm A satellite through the northern hemisphere convection zone bounded by the HMB for the corresponding statistical model. Of the 381 periods identified, 84 contained complete satellite passes. Each pass was examined by eye to ensure an offset could be chosen, based on the following requirements, to correct the Swarm ion drift measurements. Requirements include (1) the ion drift measurements be flagged as being of good quality at the HMB so that an offset could be determined accurately, and (2) the ion drift measurements be approximately constant while crossing the HMB so the offset has some degree of reliability. The along-track components for both the horizontal and vertical TII sensors were examined to determine which component was most likely to accurately reflect the true (offset) ion drift. For 14 passes, large jumps existed in the along-track data for both sensors at different times along the track. Although these jumps might have been real, the lack of corroboration between sensors made verification impossible and data from these tracks were therefore discarded. Of the 70 events remaining, the along-track component was derived from the vertical sensor for 42 events, the horizontal sensor for 2 events, and both sensors for 26 events. Data for each pass were examined in detail to remove outlying points.

The reported TII data quality flag is determined using a preliminary algorithm that evidently does not capture all outliers or problematic intervals. Therefore, each satellite pass was analyzed to identify and exclude unreliable data, which is often characterized by a double population of points in either the ion drift data or T_{ion} data, or by large ion temperatures (T_{ion} > 5000 K). Points lying more than 1 standard deviation from the mean of a 121-point boxcar average were removed, as were additional points identified by hand. Although this method certainly excludes good data as well, it provides confidence that the subsequent analysis does not include suspect data.

Procedure for correcting Swarm data

We propose correcting Swarm data by zeroing the flow at the low-latitude boundary of the convection zone (i.e., where convection is expected to be zero). Here the low-latitude boundary is defined as the HMB corresponding to the CS10 statistical convection model for the solar wind and IMF conditions that exist during the satellite pass. This is done as follows: (1) Identify the IMF and solar wind conditions for the satellite pass, and the corresponding CS10 statistical model. In this paper, we only consider satellite passes that occur during periods of quasi-stable solar wind and IMF. (2) Identify the two points where the orbital footprints of the Swarm satellite cross the HMB of the CS10 statistical model. (3) Determine the average along-track and cross-track ion drift at the intersection points identified in (2). These averages define the along-track and cross-track offsets. Note that by averaging the data at either end of the satellite pass, this method assumes stability of the offset throughout each ~20-min pass the satellite makes of the high-latitude region. Such conditions are met in this study due to the assumption of quasi-stability in the solar wind and IMF. Note that in passes where ion drifts calculated at one end of the satellite pass were contaminated by data of poor quality, then data from only the other end of the satellite pass were used as the offset value. (4) Correct Swarm ion drift measurements are carried out by subtracting the along-track offset from the along-track data and the cross-track offset from the cross-track data.

Comparison of corrected Swarm data: single satellite pass (July 4, 2014)

To illustrate the proposed procedure for correcting Swarm ion drift data, we consider a single cross-polar satellite pass. Figure 2a, b plots solar wind and IMF conditions on July 4, 2014, for a 20-min interval beginning at 07:30 UT. During this interval the IMF B_x varies

from 0 to 1 nT. IMF B_y is negative at approximately −4 nT. IMF B_z undergoes a slow variation between −1 and 1 nT until 07:40 UT and then reaches a constant value of −4 nT for the remainder of the interval. E_{sw} is constant at roughly 1.4 mV/m. Variation of the IMF and solar wind parameters are sufficiently small to classify the interval as quasi-stable based on the criteria described in "Identifying periods of quasi-stable solar wind and IMF" section. During this period the CS10 statistical model for $B_z < 0$, $B_y < 0$, $E_{sw} = [1.20, 1.70]$ mV/m, and $\beta > 10°$ is used to determine the offset in the Swarm data. The CS10 statistical model pattern has a simple two-cell configuration

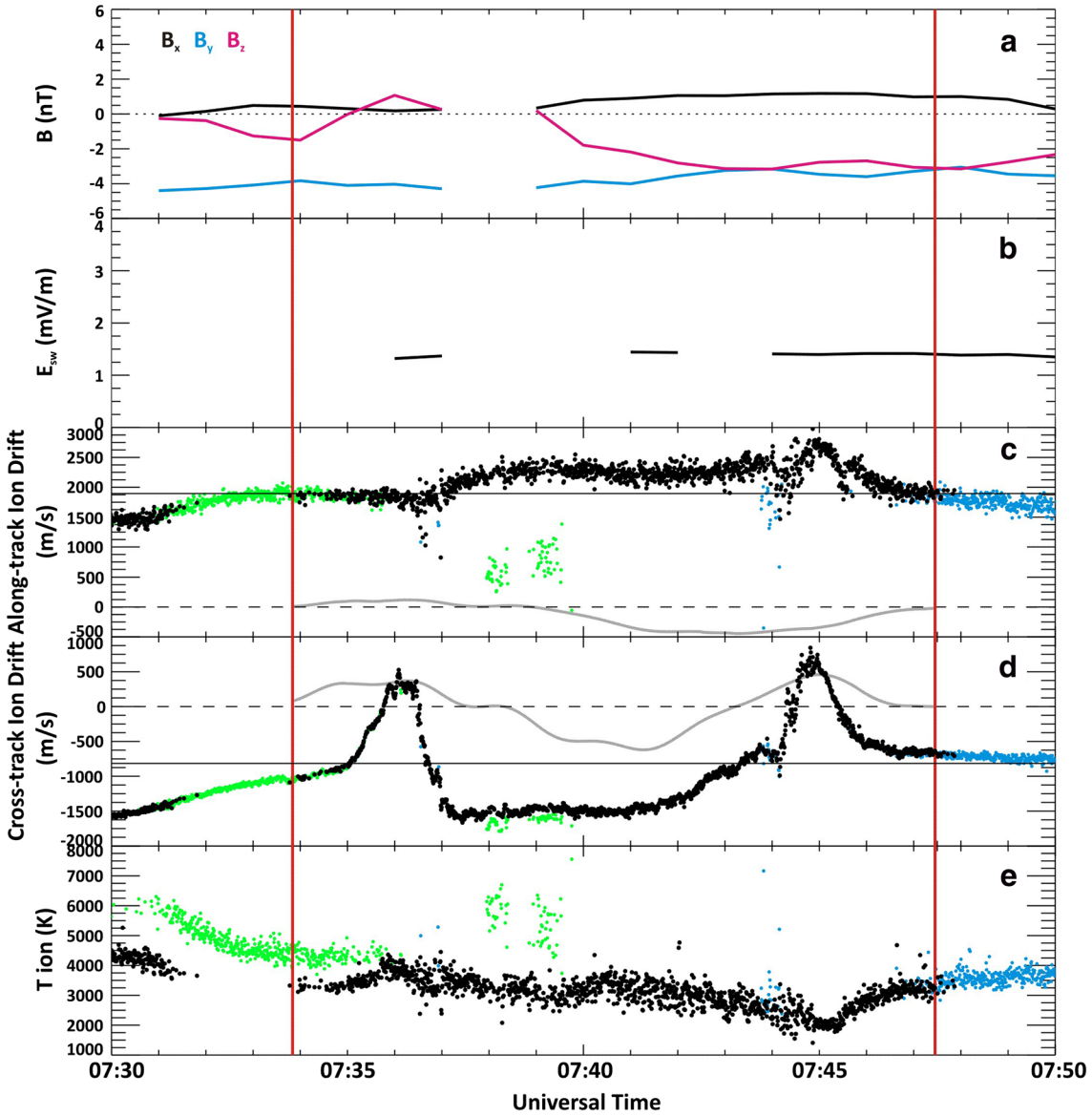

Fig. 2 Solar wind, IMF, and Swarm measurements for a single event. **a** IMF B_x (*black*), B_y (*blue*), B_z (*pink*) components, **b** solar wind electric field (E_{sw}), **c** Swarm A along-track component of the measured ion drift with satellite velocity subtracted (mean of the values measured by the horizontal and vertical sensors), **d** Swarm A cross-track component of the measured ion drift (measured by the horizontal sensor), and **e** Swarm A ion temperature (T_{ion}). In (**c**) and (**d**) the *gray line* indicates the along-track and cross-track components of the velocity for the corresponding CS10 statistical model, calculated at the coordinates of Swarm measurements within the high-latitude convection zone. In (**c**) and (**d**) the *horizontal black lines* indicate the offset used to correct Swarm ion drift data. All data are presented for the July 4, 2014, interval during which time the IMF and solar wind are in a quasi-stable state based on criteria described in "Identifying periods of quasi-stable solar wind and IMF" section. In (**c**–**e**), data flagged in the TII data file as being of poor quality are shown in *blue*, and data flagged by eye inspection as being unreliable are shown in *green*. *Vertical red lines* at 07:33:50 UT and 07:47:27 UT indicate the time at which the satellite footprints cross the HMB for the corresponding CS10 statistical model

(see Fig. 3a). During this period the Swarm A satellite makes a complete pass through the northern hemisphere high-latitude convection zone. We focus on this interval which is bounded by red vertical lines at 07:33:50 UT and 07:47:27 UT in Fig. 2.

Figure 2c, d plots the along-track and cross-track components of the measured ion drift, respectively. Data associated with a TII quality flag ≥20 are indicated in blue. The interval illustrates the need for the custom outlier removal described in "Data selection and preprocessing" section, because TII quality flag does not properly flag the outliers. Data identified as being unreliable through eye inspection are indicated in green. The remaining black points are judged to be of reliable good quality. Contributions from the satellite velocity have been removed from the along-track ion drift measurement shown in Fig. 2c. For this pass the satellite enters the convection zone at 18 MLT, crosses over the magnetic pole, and exits the convection zone at ~6 MLT; this is a dusk-to-dawn satellite pass. The measured along-track ion drift is shown to be relatively stable, entering the convection zone at 1870 m/s, exiting the convection zone at 1920 m/s and having a mean value of 2160 m/s throughout the pass.

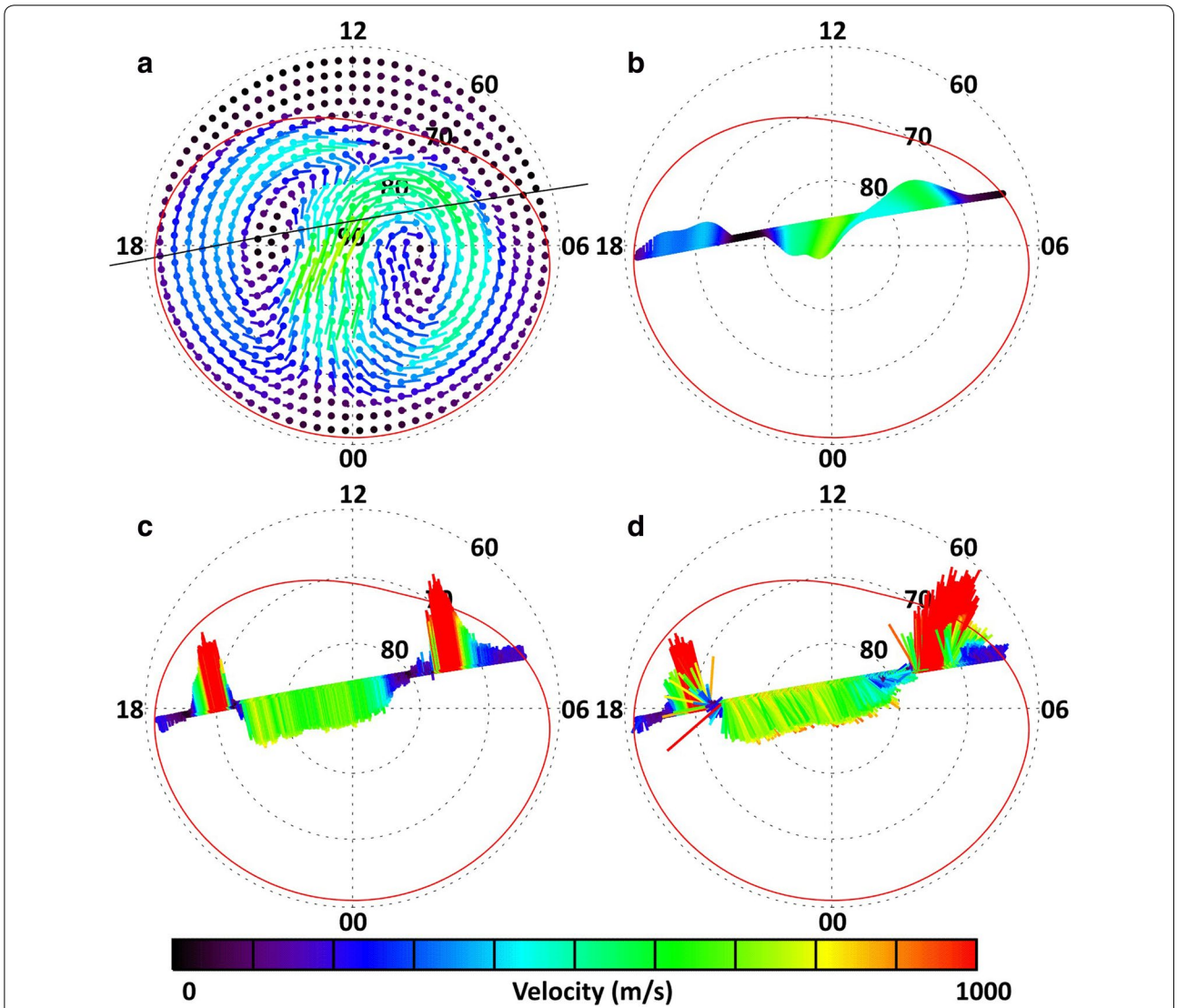

Fig. 3 Map of Swarm ion drifts for a single event. **a** The CS10 statistical model in MLAT/MLT coordinates for the northern hemisphere $B_z < 0$, $B_y < 0$, $E_{sw} = [1.20, 1.70]$ mV/m, and $\beta > 10°$, corresponding to a satellite pass on July 4, 2014. Footprints of the Swarm A satellite orbit are plotted in *black*. **b** Projection of the CS10 statistical model shown in (**a**) at coordinates of Swarm ion drift measurements. In (**c**) and (**d**) the corrected cross-track component and 2D ion drift measurements are plotted. In all plots the HMB for a minimum latitude of 61° MLAT is overplotted (*solid pink line*). Velocity magnitude is indicated by the *horizontal color bar*

The cross-track component of the measured ion drift varies in magnitude entering and leaving the convection zone at −1000 and −640 m/s, respectively. Flow reaches peaks of 530 and 840 m/s in regions which correspond to peaks in the sunward-directed return flow at the edge of the dusk and dawn convection cells. The central flow, which corresponds to anti-sunward-directed flow over the polar cap, is roughly −1500 m/s. Although such high-magnitude flows are not given by the CS10 statistical convection pattern, they are sometimes observed by instruments such as SuperDARN (i.e., Drayton et al. 2005; Parkinson et al. 2005; Koustov et al. 2006) or the DMSP satellites (Greenspan et al. 1986; Rich and Hairston 1994).

Both the along-track and cross-track components of the ion drift are expected to be zero at the low-latitude boundary of the convection zone. However, the offset is approximately 2000 m/s in the along-track direction and 600–1000 m/s in the cross-track direction. The difference in both magnitude and polarity suggests that offsets are considerably different in the along-track direction compared to the cross-track direction and therefore need to be determined separately.

Figure 2e presents the ion temperature for the July 4, 2014, event. In general, ion temperature varies smoothly within the high-latitude region, generally staying between 2000 and 5000 K. However, there are instances when there appears to be two clear populations of points: 07:30–07:36 UT, 07:38–07:40 UT intervals. Ion temperature is calculated from 4 EFI temperature estimates and such a discontinuity comes from having two separate temperature estimates. Similar discontinuities are observed in the along-track component of the ion drift reported by the vertical sensor, which are translated into the averaged along-track component plotted in Fig. 2c (07:38–07:40 UT intervals). Although it is possible for two distinct populations to exist, it is also possible that the double population of points is artificial. In such cases the grouping of points that appears to be inconsistent with the overall data set is removed prior to comparing Swarm data with the statistical model, or with data from other instruments. In cases where it is unclear which population of points should be considered, the entire period is removed.

Figure 3 maps the expected convection pattern for the July 4, 2014, interval and the corrected Swarm ion drift measurements. Figure 3a plots the CS10 statistical model corresponding to this interval, where $B_z < 0$, $B_y < 0$, $E_{sw} = [1.20, 1.70]$ mV/m, and $\beta > 10°$. Convection is two-celled with a channel of strong anti-sunward flow over the polar cap which is closed by sunward-directed flows at the equatorward edge of both the dawnside and duskside convection cells. The convection zone is bounded by the HMB which extends to 61° MLAT on the nightside. The thin black line across the plot indicates the footprints of the Swarm A satellite orbit across the high-latitude region. The average ion drift measurement at the intersection of the footprints of the satellite orbit and the HMB determines the offset used to correct the Swarm data. In Fig. 3b, the CS10 statistical model plotted in Fig. 3a is projected onto the coordinates of Swarm ion drift measurements to illustrate the expected flow. Based on the CS10 statistical model pattern, flow is expected to point in the sunward direction in the dawn and dusk regions equatorward of 75° MLAT with magnitudes of up to 300–400 m/s on the duskside and 500 m/s on the dawnside. Flow poleward of 80° is expected to point in the anti-sunward direction with magnitudes of up to 700 m/s.

To compare the measured and modeled ion drift, consider the gray lines in Fig. 2c, d, which indicate the along-track and cross-track components of the ion drift for the CS10 statistical model. In Fig. 2c, traces for the measured and CS10 model ion drift differ by as much as 2000 m/s in magnitude in the along-track direction. In the cross-track direction, the CS10 statistical model clearly illustrates the pattern of sunward-directed (positive) flow in the outer regions of the convection pattern and anti-sunward-directed (negative) flow across the polar cap. Swarm observes comparable peaks in the cross-track component at approximately the same locations as the statistical model, but the peaks are much narrower and the surrounding flow is considerably offset from the statistical model. For both the along-track and cross-track components of the ion drift, an offset in flow magnitude is apparent.

It is clear that it is necessary to make corrections to the Swarm data before it will accurately represent the true convection pattern, which for this period of quasi-stability should approximately be represented by the CS10 statistical model shown in Fig. 3a. Swarm ion drift measurements are corrected using the procedure described in "Procedure for correcting Swarm data" section. Offsets of 1895 and −820 m/s were determined for the along-track and cross-track directions, respectively. These offsets are indicated by solid thin horizontal black lines in Fig. 2c, d.

Figure 3c, d show the corrected cross-track ion drift measurement and the corrected full 2D ion drift measurement, respectively. With the exception of a region of anti-sunward-directed flow near the HMB at 18 MLT, the flow pattern demonstrated by the corrected Swarm ion drift data follows patterns established by the CS10 statistical model including anti-sunward flow over the polar cap and strong return flow in the auroral regions. The magnitude of the flow reported poleward of 80° MLAT is similar in Fig. 3a, d.

A direct comparison can be made between the measured ion drift and the statistical model. This is done by calculating the CS10 statistical model at Swarm measurement coordinates and projecting the resulting vectors into the along-track and cross-track directions so that the vector components can be examined separately. Figure 4 shows scatter plots of the measured and CS10 statistical model ion drift components both before (black points) and after (blue points) removing an offset. Prior to removing an offset, the measured along-track ion drift is clustered between 1000 and 3000 m/s whereas the CS10 model flow is constrained to −250 to 500 m/s. Removing an offset shifts the measured ion drift by 1895 m/s showing much closer agreement with the CS10 statistical model in terms of magnitude. In the cross-track direction, Swarm measures velocities spread between −1600 and 1000 m/s compared to CS10 model velocities which range from roughly −700 to 500 m/s. Data show excellent correlation with the CS10 model flow ($R = 0.80$) but are offset from the ideal bisector (dashed line) by −826 m/s. Adding an offset of 820 m/s significantly improves the comparison. Once an offset is removed, points in the cross-track plot lie almost exactly along the ideal bisector, except for Swarm flow measurements greater than ~700 m/s. In Fig. 3c such flow corresponds to the high-velocity flows (red) measured by Swarm at 70°MLAT on the duskside and 75° MLAT on the dayside.

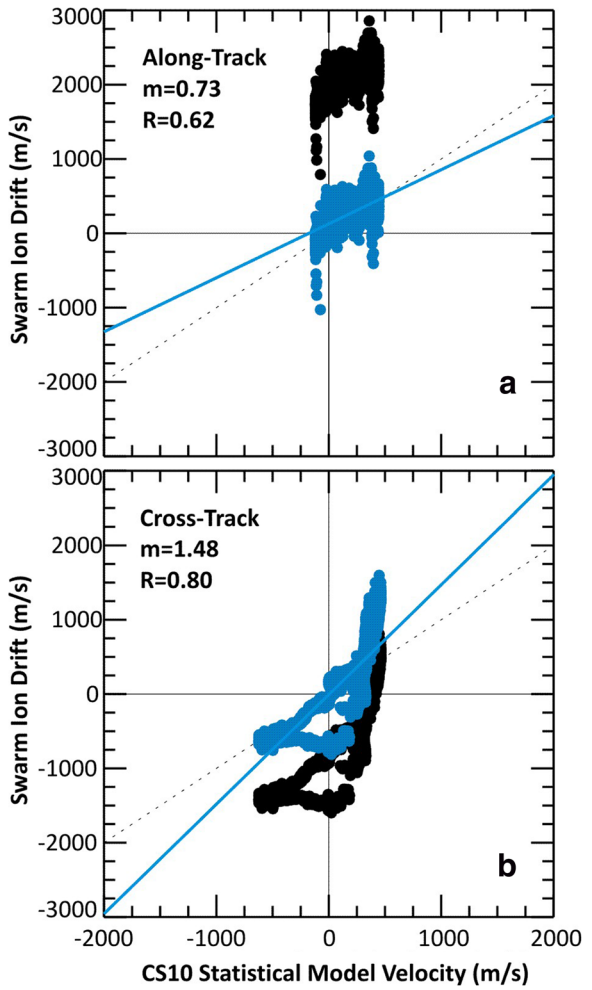

Fig. 4 Comparing Swarm and CS10 model data before/after removing an offset—single event. Comparison of the **a** along-track and **b** cross-track ion drift measured by the Swarm A satellite and the corresponding CS10 statistical models for the July 4, 2014, pass illustrated in Figs. 2 and 3. *Black* and *blue points* represent the distribution of points before and after removing an offset from the data. The best-fit line to the data (*heavy blue line*), slope (*m*) of the best-fit line, and correlation coefficient (*R*) are indicated. The *dashed line* indicates perfect agreement

Comparison of corrected Swarm data: multiple satellite passes

Swarm A satellite data for the 70 passes occurring during periods of quasi-stability were compared directly to ion drifts inferred from the CS10 statistical model before and after correcting for an offset (Fig. 5). Prior to correcting for an offset (top row in Fig. 5), the bulk of the Swarm ion drift data spans from 0 to 3000 m/s in the along-track direction and −2500 to 1500 m/s in the cross-track direction. The magnitude of the CS10 model data is strictly <1000 m/s for both components. In the along-track direction the correlation coefficient indicates poor agreement ($R = 0.16$). Correlation is somewhat better in the cross-track direction ($R = 0.40$), although again, far from ideal.

Despite performing the comparison during periods where the convection pattern is expected to be stable and agree with the statistical model, neither ion drift measurement component shows agreement with the CS10 statistical model. If the Swarm ion drift measurements were offset by a single constant background level, we would expect to see correlation (e.g., $R > 0.50$) between data sets with a disagreement in velocity magnitudes. The poor correlation illustrated in the top row of Fig. 5 therefore suggests the offset is different for each pass and needs to be independently determined for each pass.

Data in the top row of Fig. 5 clearly show the offset is different in both the along-track and cross-track directions. Consider Fig. 1b which shows the distribution of the coordinates of the satellite measurements within the HMB for the 70 satellite passes considered in this study. Satellite passes are generally oriented from dusk to dawn, and data are weighted toward the nightside. Based on the two-celled convection pattern that dominates the nightside region for both northward and southward IMFs, and the predominance of a two-celled (IMF $B_z < 0$)

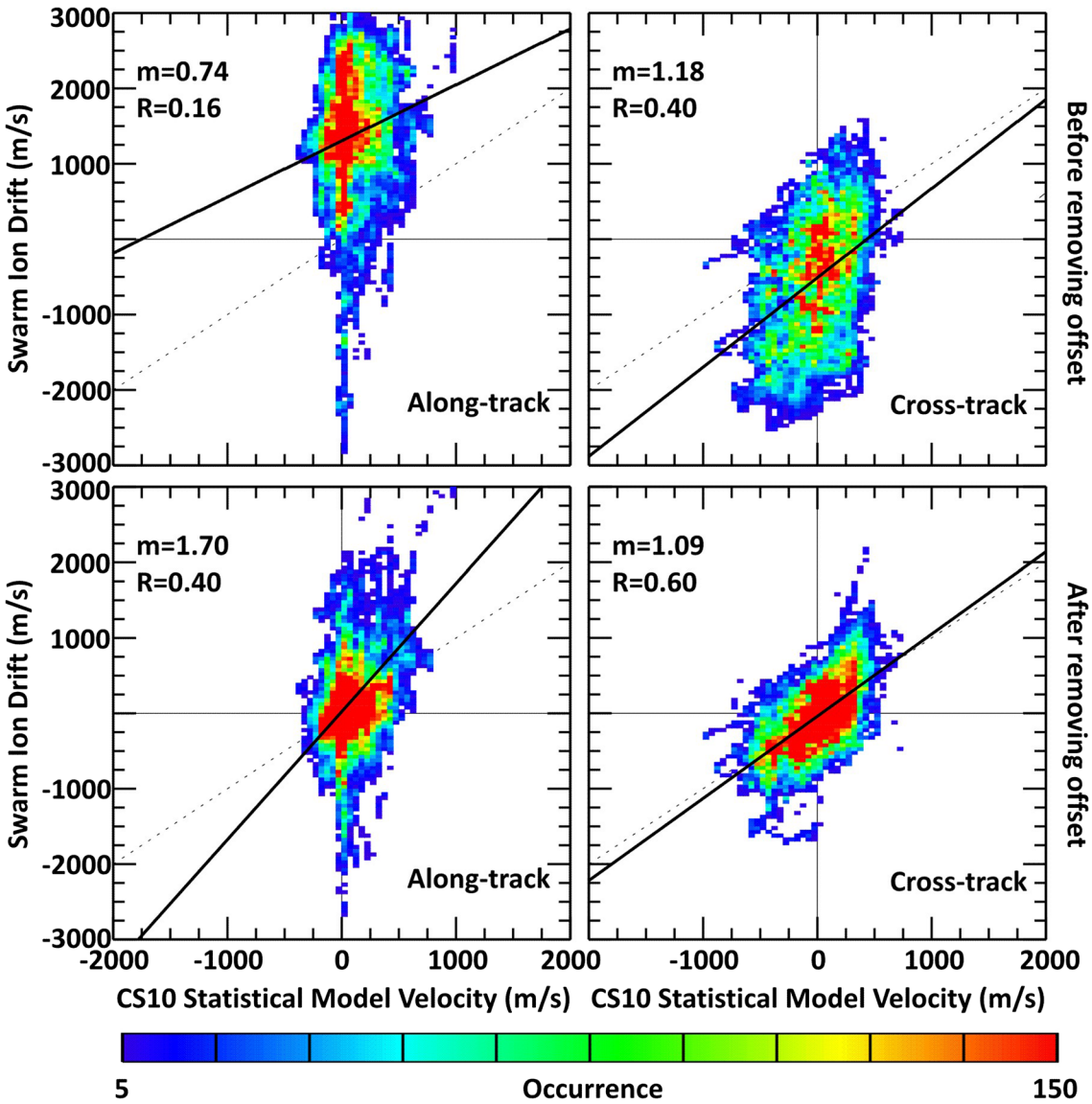

Fig. 5 Comparing Swarm and CS10 model data before/after removing an offset—multiple events. Comparison of the along-track and cross-track ion drift measured by the Swarm A satellite and the corresponding CS10 statistical models for 70 northern hemisphere passes during May–September 2014 for periods of quasi-stable IMF and solar wind. Comparisons are performed both before (*top row*) and after (*bottom row*) removing an offset from the Swarm data. Data were binned in increments of 50 m/s. The number of occurrences in each bin is indicated by *color* according to the *color bar* shown. The best-fit line to the data (*heavy black line*) and correlation coefficients are indicated. The *dashed line* indicates perfect agreement

convection pattern for the 70 events (61 events for $B_z < 0$ and 9 events for $B_z > 0$), this dusk-to-dawn orientation suggests the along-track component of the flow will be small, near zero, and the cross-track component will vary with both positive and negative values. Although data in Fig. 5 roughly follow expectations in the cross-track direction, along-track ion drifts are clustered at values much greater than zero. This suggests the offset in the Swarm data needs to be independently determined for the along-track and cross-track directions.

The method described in "Procedure for correcting Swarm data" section was used to determine offsets for the entire 70-pass data set. Figure 6 shows the distribution of offsets in the cross-track and along-track directions. The broadness of the distribution suggests that correcting the offset is not quite as straightforward as removing a single constant offset from all data. In the cross-track direction the distribution is wide, spanning from −2000 to 800 m/s with a peak in the bin centered at −300 m/s and a mean value of −470 m/s. The distribution for the along-track

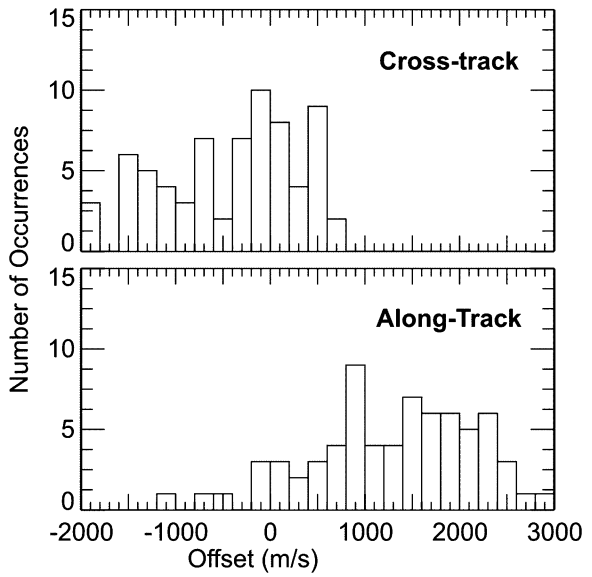

Fig. 6 Distribution of cross-track and along-track offsets. Distribution of the offset determined for the cross-track and along-track directions

direction is also wide, spanning from −1200 to 2600 m/s, peaking in the 900 m/s bin, and having a mean value of 1150 m/s. The mean offsets differ in polarity with magnitudes differing by a factor of 2.4, enforcing the notion that the along-track and cross-track components of the measured ion drift need to be handled separately. This is in fact expected since different algorithms are used to derive velocities in these two components.

The comparison between Swarm and CS10 data for the 70 identified satellite passes after removing an offset is illustrated in the bottom row of Fig. 5. Removing an offset from the measured Swarm ion drift components significantly improves the agreement between data sets. In the along-track direction Swarm ion drift measurements are centered at 0 m/s and the majority of points have magnitudes of <1000 m/s. However, the correlation coefficient is still poor ($R = 0.40$) and the slope of the best-fit line to the data ($m = 1.70$) indicates the along-track component of the measured ion drift is larger than that of the CS10 statistical model. It should be noted that despite the poor agreement indicated by R and m, the shift in the y-intercept of the best-fit line to the data from 1300 to 23 m/s is a significant improvement. Improvements in the cross-track direction are more significant with the correlation increasing to $R = 0.60$ indicating a linear relationship. However, the slope ($m = 1.09$) drops only slightly and there is still a tendency for the Swarm cross-track component of the measured ion drift to be larger than the statistical model. Removing extraneous points having magnitudes >1200 m/s reduces the slope from $m = 1.09$ to $m = 1.00$. These results, particularly for the cross-track component of the flow, are excellent when considering that the CS10 model represents the average flow rather than the true flow.

In the multi-pass data set, there is a predominance for the quasi-stable interval to have IMF $B_z < 0$: There are 9 passes for $B_z > 0$ and 61 for $B_z < 0$. If Fig. 5 is reprocessed limiting to those events where the IMF $B_z < 0$ and the convection pattern is more simple (two-celled opposed to multi-celled) then the correlation coefficient after removing an offset increases slightly from $R = 0.40$ to $R = 0.42$ in the along-track component and from $R = 0.60$ to $R = 0.63$ in the cross-track component. The slopes of the best-fit lines to the data also increase from $m = 1.70$ to $m = 1.81$ in the along-track direction, and from $m = 1.09$ to $m = 1.15$ in the cross-track direction.

To examine the MLAT and MLT location of where the data did and did not agree, the mean ($\bar{x}$) and standard deviation (σ) of the difference between the cross-track component of the CS10 statistical model, and the corrected Swarm ion drift measurement were considered. Figure 7 plots the distribution of the MLAT and MLT location of the ion drift for the entire comparison data set (black), for points of agreement (data falling within 2σ of $\bar{x}$) (blue) and for points of disagreement (data falling outside 2σ of $\bar{x}$) (red). For both MLAT and MLT, the distribution of points within 2σ of $\bar{x}$ agrees quite well with the overall distribution. For points with differences greater than 2σ of $\bar{x}$, there are additional peaks in the distributions. For the MLAT distribution, the most significant difference is a wide peak centered at 63.5° MLAT with a minor peak located at 89.5° MLAT. Additional peaks in the MLT distributions are located at 6 MLT (dawn) and 19 MLT (dusk). These distributions indicate that the largest differences between Swarm and CS10 cross-track data tend to occur over the regions of peak velocity in the sunward-directed return flow near the auroral oval, consistent with the high-velocity flows mapped in Fig. 3c, d.

As a final consideration, we bring to attention the study by Gillies et al. (2009) who point out that SuperDARN velocity measurements typically underestimate the plasma flow due to the imprecise use of a refractive index of 1 in the calculation of line-of-sight velocity. They propose a method of approximating the actual index of refraction based on the elevation angle of the returned radar signal. Using this technique they show a 12 % increase in flow magnitude. Since the SuperDARN data set used to generate the CS10 statistical model did not incorporate this correction factor, the CS10 model velocities used in this study could be underestimated by 12 %. If index of refraction considerations are applied to this study, then the slope of the best-fit line to the data in

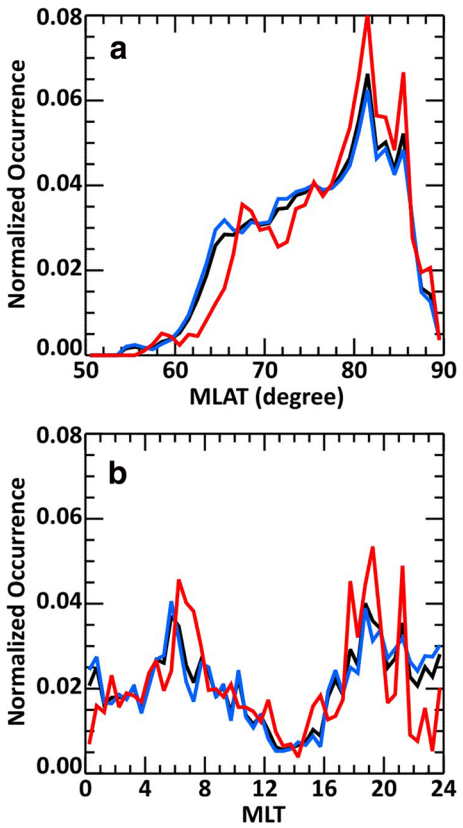

Fig. 7 MLAT and MLT location of Swarm measurement coordinates for points of good/bad agreements. Distribution of the **a** MLAT and **b** MLT coordinates of Swarm A satellite data for 70 northern hemisphere passes during May–September 2014 for periods of quasi-stable IMF and solar wind. Distributions are for all data (*black*), and data for which the difference between the measured cross-track ion drift and the corresponding CS10 statistical model was <2σ (*blue*) and >2σ (*red*) of the mean

Fig. 5 would decrease from $m = 1.70$ to $m = 1.52$ in the along-track direction and from $m = 1.09$ to near-unity at $m = 0.97$ in the cross-track direction.

Identifying boundaries in the ionospheric convection pattern based on corrected Swarm ion drift data

The convection reversal boundary (CRB) is a characteristic boundary separating anti-sunward cross-polar flow and sunward-directed return flow at auroral latitudes (Ridley and Clauer 1996; Chen et al. 2015; Koustov and Fiori 2016). The CRB is of particular interest because it is located near the ionospheric projection of the open/closed magnetic field line boundary (Sotirelis et al. 2005; Hubert et al. 2010), i.e., in the region where magnetic field lines poleward of the boundary are connected to the magnetotail lobes or the solar wind while magnetic field lines equatorward of the boundary are closed.

Accurate identification of the CRB location requires knowledge of the 2D convection pattern across the high-latitude region, particularly poleward of 70° MLAT. Due to its extensive coverage, and capability for continuous monitoring, the SuperDARN radar network is well suited for CRB mapping (e.g., Bristow and Spaleta 2013; Koustov and Fiori 2016). However, echoes are often missed in specific regions due to changing signal propagation conditions (e.g., Danskin et al. 2002). Because of this, SuperDARN convection maps often have an insufficient number of data points to overwhelm the statistical model when convection mapping and the maps therefore tend to emulate the statistical model (Mori and Koustov 2013). For this reason, satellite instruments can make a valuable contribution to mapping the CRB location, as has been demonstrated by de la Beaujardiere et al. (1991). Satellite data are useful both for instantaneous mapping concentrating in specific MLT sectors (e.g., Chen et al. 2015) and for statistical analysis (Rich and Hairston 1994), if convection is quasi-stable during the satellite pass.

We tested the ability of the Swarm A satellite to identify the CRB by considering dusk-to-dawn aligned passes for a subset of the 70 events (considered in "Comparison of Swarm data with output from a statistical convection model" section) for which the IMF B_z was negative so that the convection pattern was two-celled and well defined. For each pass the cross-track component of the corrected ion drift measurement was examined to determine the latitude at which the cross-polar cap flow reversed from having an anti-sunward-directed component to a sunward-directed component. Convection reversals were also identified in the CS10 statistical model at the same MLT location as those identified in the Swarm data. Convection reversals were found to be reliably determined for 38 passes providing a total of 42 points. Figure 8a presents the results. Black and green points indicate the CRB location determined from the CS10 statistical model and from measurements, respectively. Corresponding data for each pass are connected using a red line which indicates the latitudinal displacement of the CRB.

Data in Fig. 8a show that the CRB locations determined using both CS10 model and measured data are distributed within the same region. This indicates a general agreement in both the CRB location and the overall shape of the convection pattern, as predicted by Cousins and Shepherd (2010). Figure 8b shows the distribution of the latitudinal displacement between the CRB points identified using the CS10 statistical model and measurements. The difference in latitude is defined as negative when the CS10 model MLAT is located poleward of the Swarm MLAT and positive when the Swarm MLAT is located poleward of the CS10 model MLAT. Thirty-seven

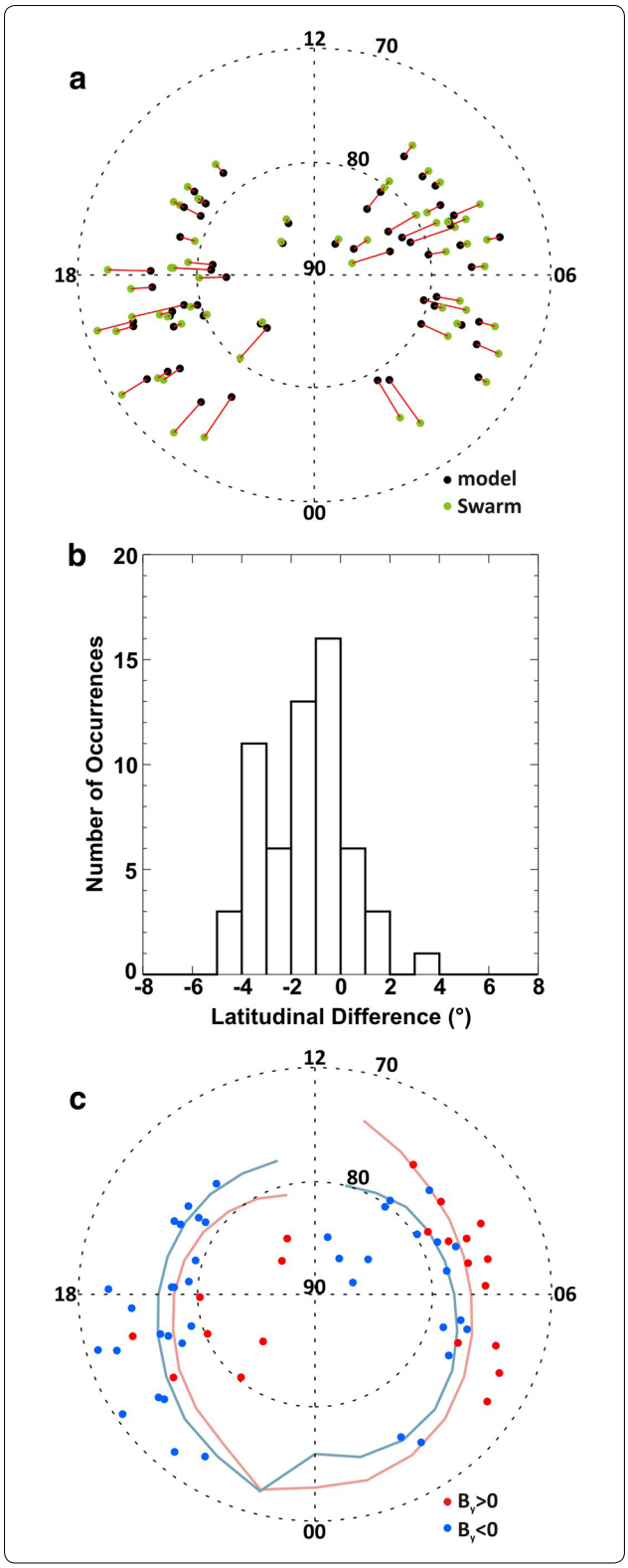

Fig. 8 Identifying the convection reversal boundary with Swarm ion drifts. **a** *Green filled circles* indicate the location of convection reversal boundary for a subset of 38 Swarm A satellite passes identified (see text) based on the cross-track component of the ion drift from the Swarm A satellite measurements. *Black filled circles* indicate the location of the CRB corresponding to the MLT of the Swarm-derived point determined for the CS10 statistical model corresponding to each pass. *Red lines* connect Swarm and CS10 points for each pass. **b** Histogram of latitudinal difference (degrees) between matching CS10 model and measured convection reversal coordinates. Angular spacing is defined as negative if the CS10 model coordinate is poleward of the Swarm coordinate and positive if the Swarm coordinate is poleward of the CS10 model coordinate. **c** *Filled circles* indicate the location of convection reversals determined from the Swarm A satellite measurements for periods of IMF $B_y < 0$ (*blue*) and IMF $B_y > 0$ (*red*). *Curves* in (**c**) represent the CRB location determined in Koustov and Fiori (2016) for IMF $B_y < 0$ (*blue*) and IMF $B_y > 0$ (*pink*) based on a statistical average of SuperDARN data for IMF $B_t = [-4, 0]$ and IMF $B_z < 0$ (their Fig. 6). All data in this figure are for periods of IMF $B_z < 0$

percentage of points are separated in latitude by <1°, and 64 % of points are separated by <2°.

Figure 8b indicates a tendency for the Swarm CRB to be located at more equatorward latitudes as compared to the CS10 statistical model. In 83 % of cases, $\mathrm{MLAT}_{\mathrm{SWARM}}$ is equatorward of $\mathrm{MLAT}_{\mathrm{CS10}}$. Averaging the MLAT location of the dawnside and duskside CRB locations for each data set also reveals a tendency for the CRB to be located at lower latitudes when identified using Swarm measurements compared to the CS10 statistical model. Based on Swarm measurements, the average MLAT of the CRB is 77.0° on the duskside and 78.1° on the dawnside. The CS10 statistical model puts the average MLAT of the CRB at 78.6° MLAT on the duskside and 79.0° MLAT on the dawnside. This systematic shift of the CRB determined by Swarm measurements to more equatorward latitudes is expected. The FIT technique (Ruohoniemi and Baker 1998) relies on an accurate selection of the low-latitude boundary of the convection zone given. In the FIT procedure, this boundary is taken to be the largest boundary containing all SuperDARN gridded line-of-site velocities that are greater than 100 m/s (Ruohoniemi and Baker 1998). Given the comparatively low number of low-latitude measurements used to generate the CS10 statistical model, it is likely that this boundary was assigned to a slightly more poleward latitude than it should be for all maps. Although this is not likely to alter flow intensity in the most equatorward region of the statistical convection model, it could prevent convection foci from shifting to more equatorward locations, thereby forcing the CRB to slightly more poleward locations.

Bristow and Spaleta (2013), Chen et al. (2015), and Koustov and Fiori (2016) all report an asymmetry in the dawn/dusk location of the CRB. We attempted to test this asymmetry by considering Swarm measurements for periods with IMF $B_z < 0$. In Fig. 8c we show the CRB location for periods where IMF $B_y < 0$ (blue points, 25

events), and for periods where IMF $B_y > 0$ (red points, 13 events). We also show here the statistically averaged CRB location inferred from SuperDARN data by Koustov and Fiori (2016). Both plots show that for periods of IMF $B_y < 0$, the duskside CRB is shifted to more equatorward latitudes and the dawnside CRB is shifted to more poleward latitudes. For IMF $B_y > 0$, the duskside CRB is shifted to more poleward latitudes and the dawnside CRB is shifted to more equatorward latitudes.

Points in Fig. 8c agree well with the average location of the CRB found in Koustov and Fiori (2016). Blue and red curves in Fig. 8c show the location of the CRB for various MLT for 228 months of observations. There is reasonable overlap between data sets, particularly on the dawnside. Note that the average curves derived by Koustov and Fiori (2016) do not reflect the very high latitude (>80° MLAT) CRB locations identified from the Swarm data. However, similar points were identified by the statistical model (see Fig. 8a). This overall agreement between the Swarm-derived data points and the blue and red curves by Koustov and Fiori (2016) indicate the Swarm-inferred CRB locations are very close to those known from SuperDARN data. Thus, the Swarm ion drift data, corrected according to the procedure proposed in this study, are in accordance with results of Bristow and Spaleta (2013), Chen et al. (2015), and Koustov and Fiori (2016), in terms of the CRB location.

Discussion

In this paper ion drift measured by the Swarm A satellite is assessed for the first time through comparison with the CS10 statistical convection model for periods of quasi-stable solar wind and IMF. Offsets in the original Swarm ion drift data were removed by zeroing each component of the measured ion drift at the equatorward edge of the convection zone as defined by the Heppner–Maynard boundary corresponding to the CS10 statistical convection model for that period. It was shown that removing these offsets significantly improves the overall agreement between measured and modeled ion drift. However, there are numerous occasions where Swarm observes large ion drifts (>1000 m/s) which are not reflected in the statistical convection model.

The disagreement between measured and modeled values can be explained in part by recalling that the CS10 statistical model presents an average convection pattern, whereas each Swarm pass represents a more dynamic 'instantaneous' (~20-min pass) measurement. Rich and Hairston (1994) observe that features regularly seen in an instantaneous convection map may not be observed in a statistical model; they specifically refer to fast flows of >1000 km/s often observed near the cusp region. They argue that such features are highly dynamic in both magnitude and location so that averaging will smooth out these features. Cousins and Shepherd (2010) agree that the ion drift reported by a statistical model will be attenuated due to the filtering and averaging performed when generating the model. However, they point out that instantaneous convection maps, and their corresponding statistical models should have the same overall configuration, the same relative difference in convection strength between cells, and fast flows should be located in the same regions. Therefore, we conclude that the practice of zeroing the Swarm ion drift data at the convection zone boundary should produce ion drifts that reflect the overall pattern of convection defined by the statistical model. One way of determining whether or not the overall shape of the convection pattern is being maintained by Swarm ion drift measurements, is to examine the location of flow boundaries, such as was done in "Identifying boundaries in the ionospheric convection pattern based on corrected Swarm ion drift data" section. Convection reversal boundaries could be identified in the corrected Swarm data and these locations agree with those predicted by the statistical model, with a 0.9°–1.6° equatorward shift in MLAT which could be at least partially attributed to the algorithm used to derive the statistical model.

Another more fundamental explanation for the differences between measured and modeled data deals with the forces driving ionospheric plasma flow. The CS10 statistical convection model is parameterized by the upstream solar wind and IMF and therefore assumes the front-side reconnection rate is the driving factor controlling the ionospheric convection pattern. The expanding/contracting polar cap (ECPC) paradigm, originally described by Siscoe and Huang (1985) and further discussed in a number of papers (i.e., Cowley and Lockwood 1992; Lester et al. 2007; Milan et al. 2012; Milan 2013), offers a more encompassing explanation for convection drivers. In the ECPC paradigm, convection flow is controlled by the addition or subtraction of magnetic flux to the polar cap due to reconnection in the magnetosphere. Dayside reconnection, controlled by the upstream solar wind and IMF, and nightside reconnection, controlled by conditions in the magnetotail and substorm processes, cause the addition and subtraction of magnetic flux, respectively. The imbalance of the short-term dayside and nightside reconnection rates leads to the expansion and contraction of the polar cap, exciting ionospheric plasma flow in an effort to return the system to an equilibrium state. Note that rates balance over the long term, but not over the short term due to the finite period of time required for information to travel from the dayside reconnection point to the nightside reconnection point.

Parameterization of the CS10 statistical model by factors driving dayside reconnection discounts the impact of nightside reconnection on convection. We expect impacts to be negligible for a period of stable solar wind and IMF, but not until solar wind and IMF conditions driving the dayside reconnection are fully communicated the nightside. We attempted to minimize impacts by discounting the first 10-minute interval of a period of quasi-stability, but Cowley and Lockwood (1992) suggest a longer delay of 30–60 min would be more accurate. To examine the impact of nightside reconnection rates on the comparisons performed in this paper, we break the data set into four regions representing the midnight (21-03 MLT), dawn (03-09 MLT), noon (09-15 MLT), and dusk (15-21 MLT) sectors. The correlation coefficient for the corrected cross-track ion drifts was lowest for the midnight sector at $R = 0.43$ and comparable in the noon, dawn, and dusk sectors averaging $R = 0.64$. Recall also that the comparison results were slightly improved for IMF $B_z < 0$ compared to IMF $B_z > 0$, possibly due to the dominance of dayside reconnection during these periods. As an additional consideration, the CRB discussed in "Identifying boundaries in the ionospheric convection pattern based on corrected Swarm ion drift data" section approximately describes the location of the open-closed field line boundary which shifts in response to the amount of magnetic flux in the polar cap. Figure 8a clearly shows that the difference between the CRB identified by data and by the CS10 model is greater on the nightside compared to the dayside; the average latitudinal difference is 1.6° on the dayside compared to 2.0° on the nightside. These results suggest that neglecting the impact of nightside reconnection in the parameterization of the CS10 statistical model impacts the agreement between measured and modeled data. In future work, we therefore recommend the use of data-driven convection patterns for identifying the convection zone boundary necessary for the offset removal described in this work.

Conclusions

Based on the work performed, a number of conclusions can be made about the quality of the high-latitude Swarm ion drift data for the May–September 2014 period:

1. There is a large discrepancy between the preliminary version (PREL 0101) of the Swarm A ion drift measurements at high latitudes (>50° MLAT) and velocities from the CS10 statistical convection models. For the entire period considered, Swarm velocity distributions peak near 2000 m/s in the along-track direction and −300 m/s in the cross-track direction whereas the CS10 statistical model velocity magnitudes are primarily <300 m/s. These results indicate there is an offset between the Swarm ion drift data and the actual drifts. The offset is different in the ion drift measured in the along-track and cross-track directions.
2. One possible method of correcting high-latitude level-1b Swarm ion drift data is to zero each velocity component at the low-latitude boundary of the convection zone. In this study, we suggested using the HMB as a proxy for the lowest latitude of the nonzero convection velocity. The CS10 statistical model was adopted to estimate the HMB location. To assess the degree of Swarm data improvement under this assumption, we selected a subset of 70 events where the IMF was quasi-stable, and the Swarm satellite made a complete pass through the northern hemisphere convection pattern. Offsets between Swarm data and CS10 predictions were determined. Removing offsets from the Swarm measurements significantly improved the agreement between measured and modeled ion drifts; the correlation coefficient increased from $R = 0.16$ to $R = 0.40$ in the along-track direction and from $R = 0.40$ to $R = 0.60$ in the cross-track direction. Agreement further improved to $R = 0.42$ in the along-track direction and $R = 0.63$ in the cross-track direction if only events with IMF $B_z < 0$ were considered.
3. The corrected Swarm data can be used to determine the convection reversal boundary location. For a subset of 38 satellite passes for periods of quasi-stable IMF and solar wind conditions where the IMF $B_z < 0$ and the satellite passed over the high-latitude northern hemisphere in a dusk-to-dawn direction, the convection reversal boundary was found to be located on average 0.9°–1.6° MLAT equatorward of the boundary predicted by the CS10 statistical model. The convection reversal boundary was shown to shift toward the dawnside or duskside depending on the polarity of IMF B_y, in full agreement with tendencies known from previous SuperDARN and DMSP measurements.

This paper demonstrates the success of removing an offset from Swarm data based on the location of the convection zone boundary as defined by a statistical model. It is recommended that in addition to performing validation work with individual instruments such as the SuperDARN radars, incoherent scatter radars, and DMSP satellites, it is highly desirable to use such instruments to generate data-driven convection patterns to more accurately determine the low-latitude boundary of the convection zone for more accurate offset removal.

Abbreviations
AACGM: altitude-adjusted corrected geomagnetic coordinates; ACE: Advanced Composition Explorer; CRB: convection reversal boundary; DE2: Dynamics Explorer 2; DMSP: Defence Meteorological Satellite Program; ECPC: expanding/contracting polar cap; EFI: electric field instrument; GSM: geocentric solar magnetospheric; H: horizontal; HMB: Heppner–Maynard Boundary; IMF: interplanetary magnetic field; LP: Langmuir probe; MLAT: magnetic latitude; MLT: magnetic local time; SuperDARN: Super Dual Auroral Radar Network; TII: thermal ion imager; V: vertical.

Authors' contributions
RADF conceived the study, processed and analyzed the Swarm ion drift data, and drafted the manuscript. AVK participated in the design of the convection reversal study and provided significant contributions in drafting the manuscript. DHB participated in the design of the study and helped draft the manuscript. DK and JKB provided the Swarm ion drift data, provided support interpreting the data, and provided feedback on the manuscript. All authors read and approved the final manuscript.

Authors' information
RADF is a research scientist for the Geomagnetic Laboratory of Natural Resources Canada specializing in space weather and ionospheric physics. She received her B.Sc., M.Sc., and Ph.D. from the University of Saskatchewan Department of Physics and Engineering Physics while studying in the Institute of Space and Atmospheric Studies. AVK teaches at the University of Saskatchewan and studies plasma flows at high latitudes with radars. DHB is head of the space weather group within the Canadian Hazards Information Service, Natural Resources Canada. DJK is in the Department of Physics and Astronomy at the University of Calgary and is the lead scientist for the Swarm EFIs. JKB is a Swarm Electric Field Instrument Scientist at the University of Calgary.

Author details
[1] Geomagnetic Laboratory, Natural Resources Canada, 2617 Anderson Road, Ottawa, ON K1A 0E7, Canada. [2] Institute for Space and Atmospheric Studies, University of Saskatchewan, 116 Science Place, Saskatoon, SK S7N 5E2, Canada. [3] Department of Physics and Astronomy, University of Calgary, 2500 University Drive, NW, Calgary, AB T2N 1N4, Canada.

Acknowledgements
This work was supported by the Natural Resources Canada, Earth Sciences Sector, Public Safety Geosciences program, the Canadian Space Agency, and the European Space Agency. Work by AVK is supported by an NSERC Grant. Comments from William Archer and Levan Lomidze regarding the Swarm EFI were appreciated. This is ESS contribution number 20150495.

Competing interests
The authors declare that they have no competing interests.

Received: 22 January 2016 Accepted: 12 May 2016
Published online: 07 June 2016

References
Archer WE, Knudsen DJ, Burchill JK, Patrick MR, St-Maurice JP (2015) Anisotropic core ion temperatures associated with strong zonal flows and upflows. Geophys Res Lett 42:981–986. doi:10.1002/2014GL062695
Baker KB, Wing S (1989) A new magnetic coordinate system for conjugate studies at high latitudes. J Geophys Res 94:9139–9143
Bhavnani KH, Hein CA (1994) An improved algorithm for computing altitude dependent corrected geomagnetic coordinates. Tech Rep PL-TR-94-2310. Phillips Laboratory, Hanscom AFB, MA, USA
Bristow WA, Spaleta J (2013) An investigation of the characteristics of the convection reversal boundary under southward interplanetary magnetic field. J Geophys Res 118:6338–6351
Chen Y-J, Heelis RA, Cumnock A (2015) Response of the ionospheric convection reversal boundary at high latitudes to changes in the interplanetary magnetic field. J Geophys Res. doi:10.1002/2015JA021024
Chisham G et al (2007) A decade of the Super Dual Auroral Radar Network (SuperDARN): scientific achievements, new techniques and future directions. Surv Geophys 28(1):33–109
Chisham G, Yeoman TK, Sofko GJ (2008) Mapping ionospheric backscatter measured by the SuperDARN HF radars—Part 1: a new empirical virtual height model. Ann Geophys 26:823–841
Cousins EDP, Shepherd SG (2010) A dynamical model of high-latitude convection derived from SuperDARN plasma drift measurements. J Geophys Res. doi:10.1029/2010JA016017
Cowley SWH, Lockwood M (1992) Excitation and decay of solar wind-driven flows in the magnetosphere–ionosphere system. Ann Geophys 10:103–115
Danskin DW, Koustov AV, Ogawa T, Nishitani N, Nozawa S, Milan SE, Lester M, André D (2002) On the factors controlling occurrence of F-region coherent echoes. Ann Geophys 20:1385–1397
de la Beaujardiere O, Alcayde D, Fontanari J, Leger C (1991) Seasonal dependence of high-latitude electric fields. J Geophys Res 96:5723–5735
Drayton RA, Koustov AV, Hairston MR, Villain J-P (2005) Comparison of DMSP cross-track ion drifts and SuperDARN line-of-sight velocities. Ann Geophys 23:2479–2486
Dungey JW (1961) Interplanetary magnetic field and auroral zones. Phys Rev Lett 6:47–48. doi:10.1103/PhysRevLett.6.47
Fiori RAD, Boteler DH, Burchill J, Koustov AV, Cousins EDP, Blais C (2013) Potential impact of Swarm electric field data on global 2D convection mapping in combination with SuperDARN radar data. J Atmos Sol-Terr Phys 93:87–99. doi:10.1016/j.jastp.2012.11.013
Fiori RAD, Boteler DH, Koustov AV, Knudsen D, Burchill J (2014) Investigation of localized 2D convection mapping based on artificially generated Swarm ion drift data. J Atmos Sol-Terr Phys 114C:30–41. doi:10.1016/j.jastp.2014.04.004
Foster JC, Holt JM, Musgrove RG, Evans DS (1986) Ionospheric convection associated with discrete levels of particle precipitation. Geophys Res Lett 13(7):656–659
Friis-Christensen E, Lühr H, Hulot G (2006) Swarm: a constellation to study the Earth's magnetic field. Earth Planets Space 58:351–358
Friis-Christensen E, Lühr H, Knudsen D, Haagmans R (2008) Swarm-an Earth observation mission investigating geospace. Adv Space Res 41:210–216
Gillies RG, Hussey GC, Sofko GJ, McWilliams KA, Fiori RAD, Ponomarenko P, St.-Maurice J-P (2009) Improvement of SuperDARN velocity measurements by estimating the index of refraction in the scattering region using interferometry. J Geophys Res. doi:10.1029/2008JA013967
Goodwin LV et al (2015) Swarm in situ observations of F region polar cap patches created by cusp precipitation. Geophys Res Lett 42(4):996–1003
Greenspan ME, Anderson PB, Pelagatti JM (1986) Characteristics of the thermal plasma monitor (SSIES) for the Defense Meteorological Satellite Program (DMSP spacecraft S8 through F10). Tech Rep AFGL-TR-86-0227 Hanscom AFB Mass
Greenwald RA et al (1995) DARN/SuperDARN: a global view of the dynamics of high-latitude convection. Space Sci Rev 71:763–796
Hairston MR, Heelis RA (1990) Model of the high-latitude ionospheric convection pattern during southward interplanetary magnetic field using DE 2 data. J Geophys Res 95(3):2333–2343
Hairston MR, Heelis RA (1995) Response time of the polar ionospheric convection pattern to changes in the north-south direction of the IMF. Geophys Res Lett 22(5):631–634
Heppner JP, Maynard NC (1987) Empirical high-latitude electric field models. J Geophys Res 92(A5):2267–4489
Hubert B, Aikio AT, Amm O, Pitkänen T, Kauristie K, Milan SE, Cowley SWH, Gérard J-C (2010) Comparison of the open-closed field line boundary location inferred using IMAGE-FUV SI12 images and EISCAT radar observations. Ann Geophys 28:883–892
Knudsen D, Burchill JK, Berg K, Cameron T, Enno GA, Marcellus CG, King EP, Weavers I, King RA (2003) A low-energy charged particle distribution imager with a compact sensor for space applications. Rev Sci Instrum 74:202–211
Knudsen D, Burchill JK, Buchert S, Coco I, Toffner-Clausen L, Holmdahl Olsen PE (2015) Swarm preliminary Plasma dataset User Note. European Space Agency SWAM-GSEG-EOPG-TN-15-0003
Knudsen DJ, Burchill JK, Buchert, SC, Eriksson A, Gill R, Wahlund J-E, Åhlen L, Smith M, Moffat B (2016) Thermal ion imagers and Langmuir probes in the Swarm electric field instruments. J Geophys Res (submitted)
Koustov AV, Fiori RAD (2016) Seasonal and solar cycle variations in the ionospheric convection reversal boundary location inferred from

monthly SuperDARN data sets. Ann Geophys 34:1–13. doi:10.5194/angeo-34-1-2016
Koustov AV, Drayton RA, Makarevich RA, McWilliams KA, St-Maurice J-P, Kikuchi T, Frey HU (2006) Observations of high-velocity SAPS-like flows with the King Salmon SuperDARN radar. Ann Geophys 24:1591–1608
Koustov AV, André D, Turunen E, Milan SE (2007) Heights of SuperDARN F region echoes estimated from the analysis of HF radio wave propagation. Ann Geophys 25:1987–1994
Lester M, Milan SE, Provan G, Wild JA (2007) Review of ionospheric effects of solar wind magnetosphere coupling in the context of the expanding contracting polar cap boundary. In: Baker DN, Klecker B, Schwartz SJ, Schwenn R, Von Steiger R (eds) Solar dynamics and its effects on the heliosphere and Earth, Space Sciences Series of ISSI vol 22, Bern, pp 117–130
Milan SE (2013) Modeling Birkeland currents in the expanding/contracting polar cap paradigm. J Geophys Res 118:5532–5542. doi:10.1002/jgra.50393
Milan SE, Gosling JS, Hubert B (2012) Relationship between interplanetary parameters and the magnetopause reconnection rate quantified from observations of the expanding polar cap. J Geophys Res. doi:10.1029/2011JA017028
Mori D, Koustov AV (2013) SuperDARN cross polar cap potential dependence on the solar wind conditions and comparisons with models. Adv Space Res 52:1155–1167
Papitashvili VO, Rich FJ (2002) High-latitude ionospheric convection models derived from Defense Meteorological Satellite Program ion drift observations and parameterized by the interplanetary magnetic field strength and direction. J Geophys Res. doi:10.1029/2001JA000264
Papitashvili VO, Rich FJ, Heinemann MA, Hairston MR (1999) Parameterization of the Defense Meteorological Satellite Program ionospheric electrostatic potentials by the interplanetary magnetic field strength and direction. J Geophys Res 104:177–184. doi:10.1029/1998JA900053
Parkinson ML, Pinnock M, Wild JA, Lester M, Yeoman TK, Milan SE, Ye H, Devlin JC, Frey HU, Kikuchi T (2005) Interhemispheric asymmetries in the occurrence of magnetically conjugate sub-auroral polarisation streams. Ann Geophys 23:1371–1390
Pettigrew ED, Shepherd SG, Ruohoniemi JM (2010) Climatological patterns of high-latitude convection in the northern and southern hemispheres: dipole tilt dependencies 219 and interhemispheric comparisons. J Geophys Res. doi:10.1029/JA014956
Reiff PH, Burch JL (1985) IMF By-dependent plasma flow and Birkeland currents in the dayside magnetosphere: 2. A global model for northward and southward IMF. J Geophys Res 90:1595–1609. doi:10.1029/JA090iA02p01595
Rich FJ, Hairston M (1994) Large-scale convection patterns observed by DMSP. J Geophys Res 99(A3):3827–3844
Rich FJ, Maynard NC (1989) Consequences of using simple analytical functions for the high-latitude convection electric field. J Geophys Res 94(A4):3687–3701
Ridley A, Clauer CR (1996) Characterization of the dynamic variations of the dayside high-latitude ionospheric convection reversal boundary and relationship to interplanetary magnetic field orientation. J Geophys Res 101:10919–10938
Ruohoniemi M, Baker KB (1998) Large-scale imaging of high-latitude convection with Super Dual Auroral Radar Network HF radar observations. J Geophys Res 103:20797–20811
Ruohoniemi JM, Greenwald RA (1996) Statistical patterns of high-latitude convection obtained from Goose Bay HF radar observations. J Geophys Res 101(A10):21743–21763
Ruohoniemi JM, Greenwald RA (2005) Dependencies of high-latitude plasma convection: consideration of interplanetary magnetic field, seasonal, and universal time factors in statistical pattern. J Geophys Res. doi:10.1029/2004JA010815
Shepherd SD, Ruohoniemi JM (2000) Electrostatic potential patterns in the high latitude ionosphere constrained by SuperDARN measurements. J Geophys Res 105(A10):23005–23014
Shepherd SG, Greenwald RA, Ruohoniemi JM (2002) Cross polar cap potentials measured with Super Dual Auroral Radar Network during quasi-steady solar wind and interplanetary magnetic field conditions. J Geophys Res. doi:10.1029/2001JA000152
Siscoe GL, Huang TS (1985) Polar cap inflation and deflation. J Geophys Res 90(A1):543–547
Sotirelis T, Ruohoniemi JM, Barnes RJ, Newell PT, Greenwald RA, Skura JP, Meng C-I (2005) Comparison of SuperDARN radar boundaries with DMSP particle precipitation boundaries. J Geophys Res. doi:10.1029/2004JA010732
Swarm Team (2004) Swarm project system requirements document for phases B, C/D, E_1. European Space Agency SW-RS-ESA-SY-001
Walker ADM, Sofko GJ (2015) Mapping steady state electric fields and convective drifts in geomagnetic fields—1. Elementary models. Ann Geophys 34:55–65. doi:10.5194/angeo-34-55-2016
Watanabe M, Sofko GJ (2009) The interchange cycle: a fundamental mode of magnetic flux circulation for northward interplanetary magnetic field. Geophys Res Lett. doi:10.1029/2008GL036682
Weimer DR (1995) Models of high-latitude electric potentials derived with a least error fit of spherical harmonic coefficients. J Geophys Res 100(A10):19595–19607
Weimer DR, King JH (2008) Improved calculations of interplanetary magnetic field phase front angles and propagation time delays. J Geophys Res. doi:10.1029/2007JA012452
Zhang S-R, Holt JM, McCready M (2007) High latitude convection based on long-term incoherent scatter radar observations in North America. J Atmos Solar Terr Phys 69:1273–1291